Gas and Solids Mixing in a Turbulent Fluidized Bed

Bing Du, Liang-Shih Fan, Fei Wei, and W. Warsito
Dept. of Chemical Engineering, The Ohio State University, Columbus, OH 43210

Gas and solids mixing characteristics in the bubbling and turbulent regimes of a gas-solid fluidized bed are examined using helium and phosphor tracer techniques to obtain the gas and solids dispersion coefficients, respectively. The real time, quasi-3-D flow behavior is qualified and quantified by the electrical capacitance tomography (ECT) technique. The mixing behavior varies significantly with the flow regimes. As the gas velocity increases, axial and radial gas dispersion coefficients increase in the bubbling regime, reach a peak at U_c, the transition velocity from the bubbling to turbulent regimes, and then decrease. In contrast, as the gas velocity increases, axial and radial solids dispersion coefficients increase in the bubbling regime and continuously increase through U_c to the turbulent regime. Temperature and pressure have little effect on the gas and solids mixing behavior. A small quantity of fine particles is noted to drastically affect the gas and solids mixing behavior in the turbulent fluidized bed. The axial and radial dispersion coefficients of gas and solids reach their maximum when the fines content is about 15%. The ECT measurements illustrate the effect of adding fines on the flow behavior in the bed. A small quantity of fine particles disintegrate the bubble/void phase, significantly modifying bubble/void- and emulsion-phase mixing behavior.

Introduction

The state of fluidization begins at the minimum fluidization velocity U_{mf}. Then the gas-solid fluidization goes through the bubbling regime, the turbulent regime, and the fast fluidization regime with increasing gas velocity. It is demarcated by the transition velocity from the bubbling to the turbulent regime U_c, and the transport velocity from the turbulent to the fast fluidization regimes U_{tr}. A number of commercial gas-solid fluidized-bed reactors that carry out chemical reactions, such as Fischer-Tropsch synthesis, acrylonitrile production, FCC regeneration, and silicon chloridization, are routinely operated in the turbulent fluidization regime. This regime offers distinct operational advantages over the bubbling and fast fluidization regimes, such as vigorous gas-solids contacting, high solids holdup, high exchange rate of the gas between the void and the emulsion phases, and relative spatial uniformity in flow properties. Understanding the gas and solids mixing behavior is important for the quantification of the reactant conversion in a fluidized-bed reactor. While the gas and solids mixing have been extensively investigated for the bubbling fluidized bed and the circulating fluidized bed, few studies address the turbulent fluidized bed.

Bi et al. (2000) presented a thorough review on the gas and solids mixing in a turbulent fluidized bed. There are some studies that investigated the axial gas mixing in turbulent fluidized beds using unsteady-state or steady-state techniques with such tracer gases as H_2, CO_2, Ar, He, CH_4 or flue gas (Cankurt and Yerushalmi, 1978; Li and Weinstein, 1989; Lee and Kim, 1989; Li and Wu, 1990; Wei et al., 1993; Foka et al., 1996). These studies indicate that the axial dispersion coefficient substantially decreases as the gas velocity increases beyond the bubbling regime. While, for turbulent fluidized beds, almost all gas mixing studies have been concentrated on the axial mixing, very limited information is available regarding the radial gas mixing. Using the steady-state CO_2 tracer gas injection, Lee and Kim (1989) investigated both the axial and radial gas mixing in the slugging and turbulent fluidized beds using Group B particles. The radial dispersion coefficient is found to increase significantly with the gas velocity in the turbulent regime. However, little is known regarding the radial gas mixing for Group A particle systems.

Correspondence concerning this article should be addressed to L.-S. Fan.

Various types of tracers have been used to measure the solids mixing in gas-solid fluidized beds, such as the salt particle tracer, ferromagnetic tracer, radioactive tracer, and phosphor tracer. Avidan and Yerushalmi (1985) used the ferromagnetic tracer to study the solids mixing of Group A particles in the bubbling, slugging, and turbulent fluidization regimes. Assuming the relatively homogeneous behavior in the turbulent fluidization regime, a one-dimensional (1-D) dispersion model was used to characterize the axial dispersion coefficient. Compared with the data from different sizes of fluidized beds, the axial dispersion coefficient increases with the square root of the bed diameter. Using a sampling technique, Wei et al. (1993) studied the solids mixing in a commercial FCC regenerator and arrived at a similar result. Lee and Kim (1990) used the steady-state axial heat flow technique to investigate the axial solids mixing for Group B particles in a turbulent fluidized bed. The axial dispersion coefficient increases with the gas velocity due to the bubble induced rapid movement of the solids. The axial dispersion coefficient of coarse particles is lower than that of fine particles, which is in part due to the high solids holdup in the bubble wake, turbulence mixing, and disintegration of fine particle clusters. Mostoufi and Chaouki (2001) studied the local axial and radial solids mixing by radioactive particle tracking. They found that both the axial and radial particle diffusivities increase with the superficial gas velocity and linearly correlate with the axial solid velocity gradient. All the studies on the solids mixing are concentrated on axial mixing or local mixing, and little is conducted on the radial solids mixing.

The gas phase in a turbulent fluidized bed occurs mainly as voids. Both the gas and solids mixing are directly related to the flow behavior of the voids. Therefore, investigating the void/bubble breakup mechanism and the void flow behavior is the key to the understanding of the gas and solids mixing in a turbulent fluidized bed. The development of a real time, high resolution process tomography provides a unique capability in assessing the internal flow behavior of a fluidized bed. The process tomography is a nonintrusive technique that utilizes remote sensors to obtain field images and then reconstruct the field based on these images. A number of tomography techniques such as X-ray, γ-ray, optical, ultrasonic, electrical, and nuclear magnetic resonant systems, have been developed and applied to study the complex multiphase phenomena (Beck and Williams, 1996; Kumar et al., 1997; Warsito et al., 1999; George et al., 2000). The electrical capacitance tomography is one of a handful of tomography techniques that can be used for real-time ($\sim$ 100 Hz) imaging of the two- or three-phase flow field (Wasito and Fan, 2001). Recently, this technique was applied for imaging gas-solid flow systems including bubbling beds, circulating fluidized beds, cyclone diplegs, and pneumatic conveying (Dyakowski et al., 1997, 2000; Yang and Liu, 2000; Smolders et al., 2001). Little is reported on the imaging of the turbulent fluidized beds.

Most commercial fluidized beds are operated in the turbulent fluidization regime at high temperatures and pressures. Many studies have indicated the effects of temperature and pressure on the transition velocity U_c, bubble size, and bubble rising velocity (Cai et al., 1989). The information on the temperature and pressure effects on the gas and solids mixing remains unclear. The addition of a small quantity of fine particles to a bed of fluidized coarse particles is known to yield significant effects on the performance of a fluidized bed such as enhancing mass and heat transfer, controlling the residence time of coarse particles, enhancing solids mixing, and increasing the reactant conversion. Sun and Grace (1990) studied the effect of three sets of particle size distributions, that is, wide, narrow, and bimodal, on the performance of a catalytic fluidized-bed reactor using ozone decomposition as a model reaction. They found that the wide size distribution yields the highest reactant conversion. The fundamental understanding of the role that fines play in determining the transport properties of the bed, such as gas and solids mixing, is thus important.

Almost all the above noted studies on gas and solids mixing were conducted at ambient conditions. It is of interest to know how the mixing characteristics vary with the temperature, pressure, and fines addition in a turbulent fluidized bed. The objective of this study is to examine the axial and radial mixing behavior of gas and solids in a fluidized bed under the high temperature and pressure conditions with fines addition. To substantiate the analyses of the gas and solids mixing behavior in the bubbling and turbulent fluidization regimes, the electric capacitance tomography is used to shed light on the real-time flow behavior.

Experimental Studies

Experimental setup

The high temperature up to 435°C and pressure up to 3.5 atm fluidized-bed system shown in Figure 1 is used in this study. The fluidized bed consists of a stainless steel column of 0.203 m ID and 2.5 m in height, a primary air heater, heating bands and a gas-solid separator placed inside the bed. A sintered stainless steel sheet with a pore size of 20 μm and fractional free area of 60% is employed as a distributor. Air from a gas compressor is first heated to a desired temperature by a primary air heater, and then introduced into the fluidized bed. Six heating bands wrapped around the column are used to maintain the fluidized-bed temperature. In the freeboard region, air and entrained particles enter a two-stage

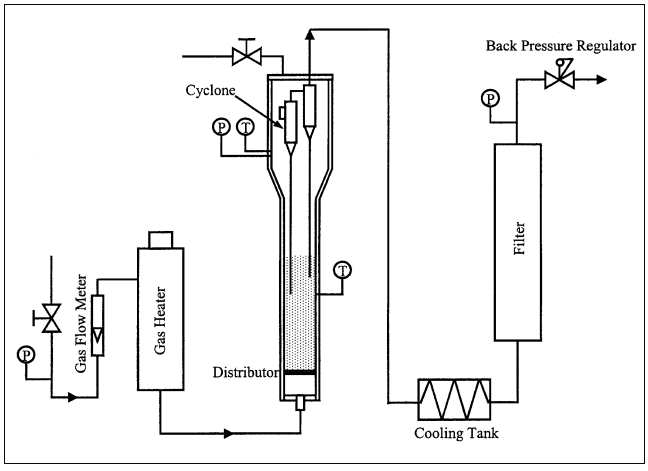

Figure 1. Fluidized-bed system.

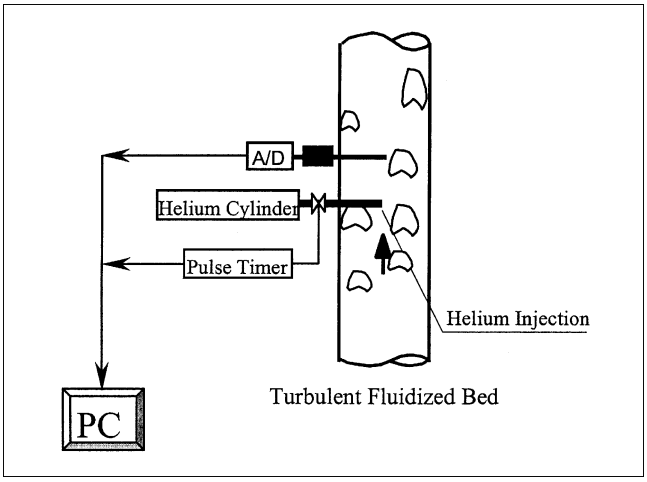

Figure 2. IHTT.

cyclone where gas and particles are separated. Particles then return to the bed. Air flows out through the cooling tank and the filter. The system pressure is regulated by a back pressure regulator installed downstream. The fluidization quality is monitored by the pressure drop and pressure fluctuation measurement.

There are ten pressure taps at a 76 mm interval along the column. The first pressure tap is located 76 mm above the distributor. A differential pressure transducer is installed to measure the pressure drop and, hence, the associated average voidage of the fluidized bed. FCC catalyst with a mean diameter of 60 μm and particle density of 1,400 kg/m^3 is used as fluidized particles (phosphor particles with similar size and density are used in the solids mixing measurement). The FCC particles with a mean diameter of 25 μm and particle density of 1,400 kg/m^3, referred to as the fine particles, are also used in the experiment. The superficial gas velocity is varied from 0.2 to 1.5 m/s, covering both the bubbling and turbulent fluidization regimes.

Impulse helium tracer technique (IHTT)

An impulse helium tracer technique is used to obtain the axial and radial gas dispersion coefficients in a turbulent fluidized bed. The tracer technique is illustrated in Figure 2. The technique includes tracer injection and detection. The tracer injector consists of a pulse timer and a pipe of 4 mm ID. The tracer flow is controlled by an electromagnetic valve and a rotameter. The tip of the tracer injector is located at the center of the bed, 0.38 m above the distributor. The tracer detector consists of a sampling probe of 1.5 mm ID, with the tip covered by a wire mesh to prevent solids ingress into the measurement system, and a thermal conductivity detector (TCD). The tracer detector is located at 76 mm, 152 mm, and 304 mm downstream, and 76 mm upstream of the tracer injector. Initially, under the control of the pulse timer, a controlled volume of helium gas is introduced into the axis of the bed. Continuous sampling of the gas takes place by a sampling probe with online TCD sample analysis. The acquisition of the time varied tracer concentration is made by the computer. The sampling probe can move along both the axial and radial directions to obtain the point tracer responses at different locations of the bed. The length of the pulse timer is set at 30 ms to guarantee a δ-function tracer injection. It is known that the sampling flow rate has little effect on the tracer concentration measurement as long as the flow rate keeps constant for each run of the experiments (Wei et al., 1994). In this study, the sampling rate is set at 40 mL/min, and the output signal is sampled at 40 Hz.

Steady-state helium tracer technique (SSHTT)

A steady-state helium tracer technique is used to substantiate the prediction of the steady-state axial and radial tracer concentration distribution based on the two-dimensional (2-D) dispersion model with the axial and radial dispersion coefficients quantified by the IHTT. The diagram of the SSHTT is almost the same as the IHTT, as shown in Figure 2. The difference is in that tracer (helium gas) is injected into the center of the bed continuously at a fixed flow rate of 3.78 L/min from the helium cylinder, and the tracer concentration is detected by the TCD under the steady state. Tracer gas is injected at 0.38 m above the distributor, and detected at 76 mm and 152 mm downstream and 76 mm upstream of the tracer injector. The sampling rate is set at 40 mL/min. For each run, the output signal for sampling is selected with a frequency of 4 Hz for a period of 5 min.

Impulse phosphor tracer technique (IPTT)

The axial and radial solids mixing behavior is measured by an impulse phosphor tracer technique. This technique is given in Figure 3. This technique employs the characteristic of the phosphorescent material that becomes fluorescent for a short period of time after being excited. The phosphor particles used in this study are produced by blending pure phosphor powder with alumina powder, which yields composite particles with size and density similar to those of FCC particles. The entire bed is made up of phosphor particles. The pulse tracer generator is a flash tube located at the center of the bed, 0.38 m above the distributor. The tracer detector con-

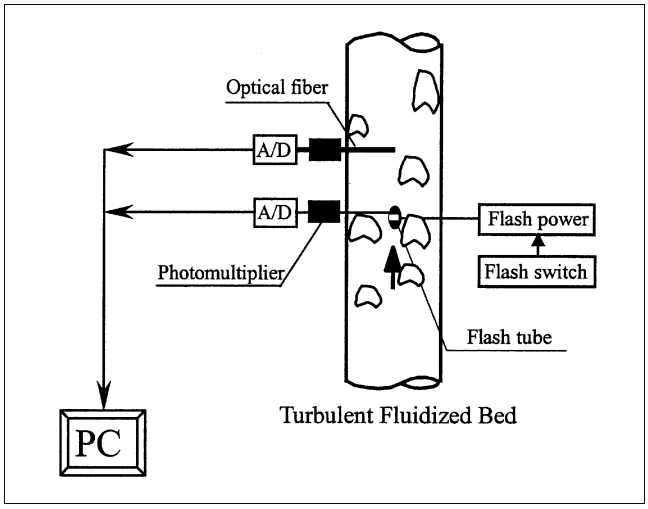

Figure 3. IPTT.

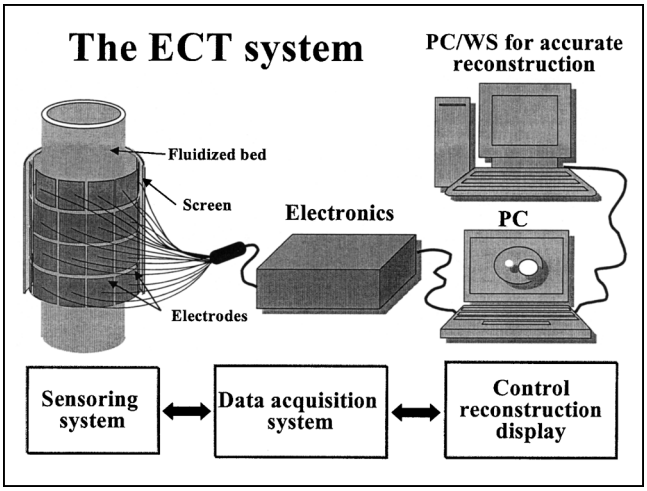

Figure 4. ECT system.

sists of an optical fiber and a photomultiplier. As shown in Figure 3, when the flash power is turned on, the flash tube gives out an impulse of strong light. Only the portion of the phosphor particles surrounding the flash tube is then excited and starts to emit light; they serve as tracer particles. The whole process of the tracer injection can be treated as a pulse since the flashing time is very short. When the tracer particles pass by the detector, the light emitted by the tracer particles is received by the optical fiber and transmitted to the photomultiplier where the tracer concentration is quantified. The advantages of this technique include ease in introducing pulse tracer particles, as well as fast on-line detection of fluorescent particles.

The tracer concentration is proportional to the light strength emitted by tracer particles. Since the emissive light from the phosphor particles decays with time, the light decay must be considered when calculating the tracer concentration. The tracer detector is located at 76 mm and 152 mm downstream of the tracer injector. The optical fiber can move along the radial positions for radial tracer concentration measurement. Another light detector is placed near the flash tube for the purpose of determining the start time of the experiment.

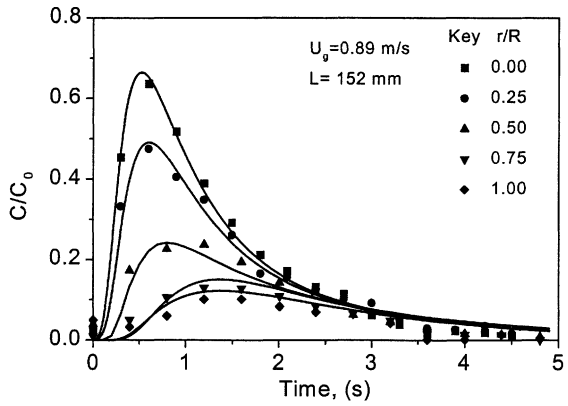

Figure 5. Typical point tracer response based on IHTT.

Electrical capacitance tomography (ECT)

The electrical capacitance tomography (ECT) system is illustrated in Figure 4. The system comprises a capacitance sensor, sensing electronics for data acquisition and a computer system for image reconstruction, interpretation, and display. The capacitance sensor array consists of a twin-plane sensor using 12 electrodes for each plane attached to the outside of the column wall, but 10 and 15 cm above the distributor for planes 1 and 2, respectively. The length of each electrode is 5 cm. Two guard sensor planes are located below and above the measuring sensor planes to adjust the electrical field within the sensoring area. There are 66 combinations of independent capacitance measurements between electrode-pairs from 12 electrodes. To qualify and quantify the flow behavior of the system, a data acquisition system, manufactured by Process Tomography Limited (U.K.), is employed for capturing the images at 100 frames per second. A neural network multicriteria optimization image reconstruction technique (NN-MOIRT) developed by Warsito and Fan (2001) is applied as the reconstruction algorithm. This technique combined a multicriterion optimization image reconstruction technique for linear tomography and a linear back projection (LBP) commonly used for capacitance tomography. Details on this technique and image reconstruction algorithm have been described elsewhere (Warsito and Fan, 2001).

Approaches

Gas mixing behavior

Figure 5 shows the typical point tracer response curves based on the IHTT. The highest concentration for the tracer response curves at a given time occurs in the axis of the column. At a given time, the tracer concentration decreases along the radial direction. With the point-source tracer injection, the radial dispersion is reflected by the differences among the peak heights of the curves at different radial positions. The axial dispersion is characterized by the width of the curves and the time when the peak is reached. The gas mixing data can be described by the dispersion model, which is characterized by the dispersion coefficient in either axial and/or radial directions. In this study, the experimental data of gas mixing based on the IHTT are analyzed by the 2-D unsteady-state dispersion model. This model assumes an upward plug flow of gas with superimposed dispersion in both axial and radial directions. A mass balance over a differential element of the column at unsteady state leads to the following equation

$$D_{a,g}\frac{\partial^2 C}{\partial x^2}+\frac{D_{r,g}}{r}\frac{\partial}{\partial r}\left(r\frac{\partial C}{\partial r}\right)-V_g\frac{\partial C}{\partial x}=\frac{\partial C}{\partial t} \qquad (1)$$

with boundary and initial conditions

$$r=R, \qquad \frac{\partial C}{\partial r}=0$$

$$r=0, \qquad \frac{\partial C}{\partial r}=0$$

$$x=-\infty, \qquad C=0$$

$$t=0,\ x=0,\ r=0, \qquad C=C_0\delta(t)$$

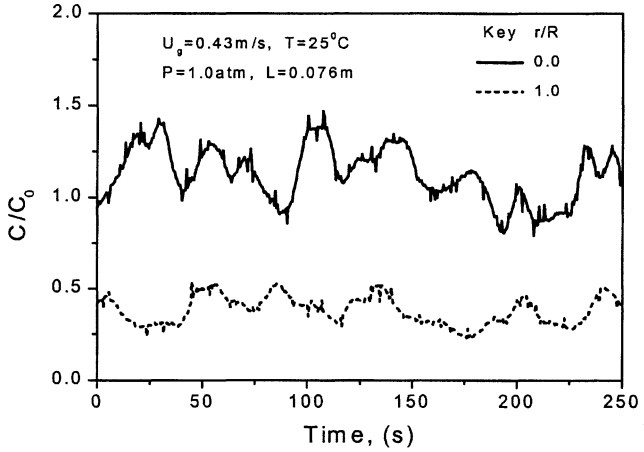

Figure 6. Tracer concentration under SSHTT.

The analytical solution for the equation (V_g = constant) can be expressed by

$$\frac{C}{C_0} = \frac{e^{\varphi\xi}}{2\pi\sqrt{\pi\theta}} \sum_{n=0}^{\infty} \frac{J_0(\beta_n \rho)}{J_0^2(\beta_n)} \exp\left[-\frac{\xi^2}{4\theta} - (\varphi^2 + \beta_n^2)\theta\right] \qquad \xi \geq 0 \quad (2)$$

$$\frac{C}{C_0} = \frac{e^{\varphi\xi}}{2\pi\sqrt{\pi\theta}} \sum_{n=0}^{\infty} \frac{J_0(\beta_n \rho)}{J_0^2(\beta_n)} \exp\left[\frac{\xi^2}{4\theta} + (\varphi^2 + \beta_n^2)\theta\right] \qquad \xi \leq 0 \quad (3)$$

The axial and radial gas dispersion coefficients $D_{a,g}$ and $D_{r,g}$ are determined using a nonlinear regression technique which minimizes the deviation between the measured point tracer response curves at various radial positions and the calculation by Eqs. 2 and 3. The solid lines in Figure 5 are the calculated results based on the 2-D dispersion model with the values of $D_{a,g}$ and $D_{r,g}$ determined in this manner. The figure shows that a good curve fitting is achieved for a given $D_{a,g}$ and $D_{r,g}$ combination.

Verification of $D_{a,g}$ and $D_{r,g}$ values based on data from SSHTT

The time series tracer concentrations measured by the SSHTT are seen in Figure 6. The curves reflect two mixing mechanisms in a fluidized bed: one is due to the bubble-induced large-scale mixing and the other is due to the small-scale gas dispersion. There is a similarity of the variation of the standard deviations of the tracer concentration fluctuations and of the pressure fluctuations with the gas velocity (Cai et al., 1989), as shown in Figure 7. It is found that the standard deviation increases with the gas velocity in the bubbling regime, reaches a maximum at the transition velocity U_c, and then decreases with increasing gas velocity in the turbulent regime. It is known that the transition from bubbling to turbulent regimes is characterized by the fact that large bubbles break up to small voids (Cai et al., 1992). This similarity shows that the tracer concentration fluctuations can also be used to determine the transition velocity U_c.

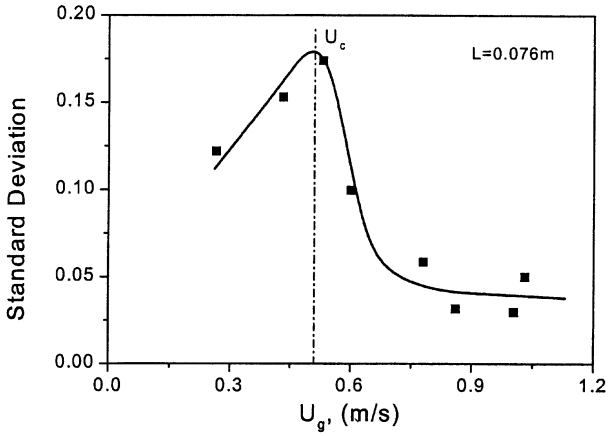

(a) Tracer concentration fluctuations based on SSHTT

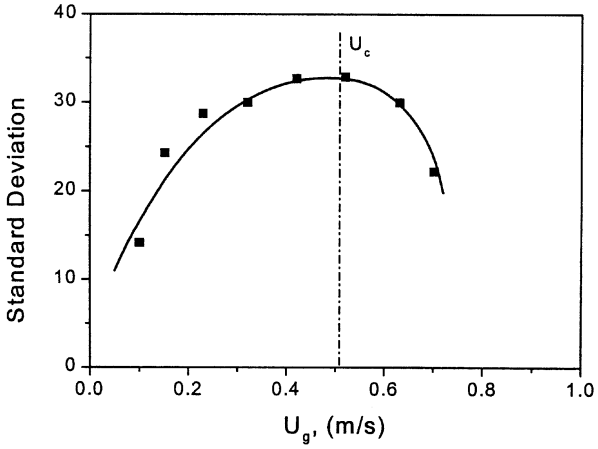

(b) Pressure fluctuations (Cai et al., 1989)

Figure 7. Standard deviation of tracer concentration and pressure fluctuations.

Figure 8 shows a series of representative time-averaged tracer concentration profiles at various radial positions based on the SSHTT. It is of a parabolic shape with a maximum

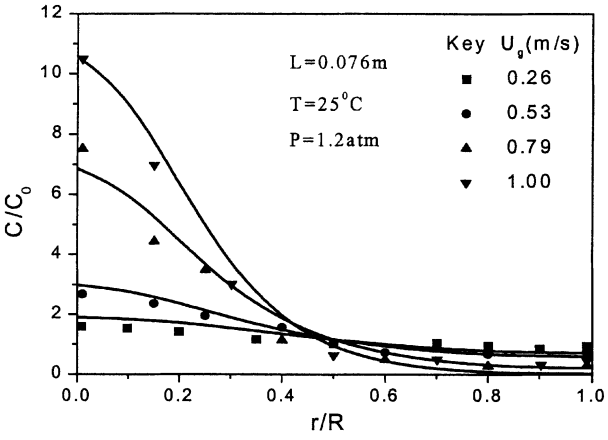

Figure 8. Prediction of steady-state experimental data based on the dispersion model.

located at the center of the bed. This pattern of profile, which suggests a convective and diffusive process for tracer propagation, is similar to that reported by Baerns et al. (1963) and Yang et al. (1993) for the bubbling and circulating fluidized beds, respectively. The effect of the gas velocity on the tracer concentration profiles is also shown in Figure 8. The tracer concentration profiles become steeper when the gas velocity increases.

Similar as the IHTT, the results of gas mixing based on the SSHTT can also be described by the 2-D dispersion model. Under steady state, Eq. 1 can be reduced to

$$D_{a,g}\frac{\partial^2 C}{\partial x^2}+\frac{D_{r,g}}{r}\frac{\partial}{\partial r}\left(r\frac{\partial C}{\partial r}\right)-U_g\frac{\partial C}{\partial x}=0 \qquad (4)$$

With the same boundary conditions as used for the IHTT, the analytical solution can be expressed by (Klinkenberg et al., 1953)

$$\frac{C}{C_0}=\varphi\sum_0^\infty \frac{J_0(\beta_n\rho)\exp\left[-\xi\left(-\varphi+\sqrt{\varphi^2+\beta_n^2}\right)\right]}{J_0^2(\beta_n)\sqrt{\varphi^2+\beta_n^2}} \qquad \xi\geq 0 \qquad (5)$$

$$\frac{C}{C_0}=\varphi\sum_0^\infty \frac{J_0(\beta_n\rho)\exp\left[\xi\left(\varphi+\sqrt{\varphi^2+\beta_n^2}\right)\right]}{J_0^2(\beta_n)\sqrt{\varphi^2+\beta_n^2}} \qquad \xi\leq 0 \qquad (6)$$

To substantiate the accuracy of the axial and radial dispersion coefficients $D_{a,g}$ and $D_{r,g}$ obtained by the IHTT, the steady-state dispersion model with $D_{a,g}$ and $D_{r,g}$ obtained by the IHTT is used to account for the experimental data of the tracer concentration based on the SSHTT. Matching both techniques is satisfactory, as shown in Figure 8.

Solids mixing behavior

The typical point tracer response curves of solids are shown in Figure 9. The tracer concentration levels off as time progresses, which agrees with the results of Avidan and Yerushalmi (1985). Similar to the experimental data of gas mixing based on the IHTT, the peak height of the curves gradually decreases along the radial position. With the point source tracer injection, the axial and radial solids dispersion is characterized by the shape of the curves and the differences among the peak heights of the curves at different radial positions, respectively. The 2-D unsteady-state dispersion model for the gas dispersion can be applied to describe the solids mixing behavior. The equation is given by

$$D_{a,s}\frac{\partial^2 C}{\partial x^2}+\frac{D_{r,s}}{r}\frac{\partial}{\partial r}\left(r\frac{\partial C}{\partial r}\right)-U_p\frac{\partial C}{\partial x}=\frac{\partial C}{\partial t} \qquad (7)$$

With the same boundary conditions as those for the IHTT,

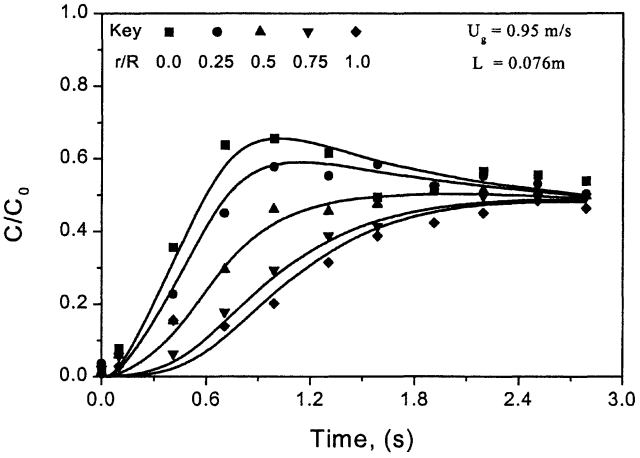

Figure 9. Typical point tracer response curves based on IPTT.

the solution is given by

$$\frac{C}{C_0}=\frac{e^{\varphi\xi}}{2\pi\sqrt{\pi\theta}}\sum_{n=0}^{\infty}\frac{J_0(\beta_n\rho)}{J_0^2(\beta_n)}\exp\left[-\frac{\xi^2}{4\theta}-\left(\varphi^2+\beta_n^2\right)\theta\right] \qquad (8)$$

The axial and radial solids dispersion coefficients $D_{a,s}$, $D_{r,s}$, and the tracer particle velocity U_p are determined by means of a nonlinear regression technique which minimizes the deviation between the measured point tracer response curves at various radial positions and the calculation by Eq. 8. As shown in Figure 9, the solid lines predicted by this 2-D dispersion model fit the experimental data well, which indicates the accuracy of the obtained values of $D_{a,s}$, $D_{r,s}$, and U_p.

Figure 10 shows the averaged tracer particle velocity U_p predicted by the dispersion model. In a bubbling or turbulent fluidized bed, the flow pattern of the solids phase is composed of the gross circulation of particles and the local solids movement. The averaged particle velocity is small and is determined by the extent of particle entrainment. As shown in Figure 10, U_p is of the order of 0.001 m/s and increases with the gas velocity. Also shown in the figure are the calculated values using the correlation of Tasirin and Geldart (1998). It

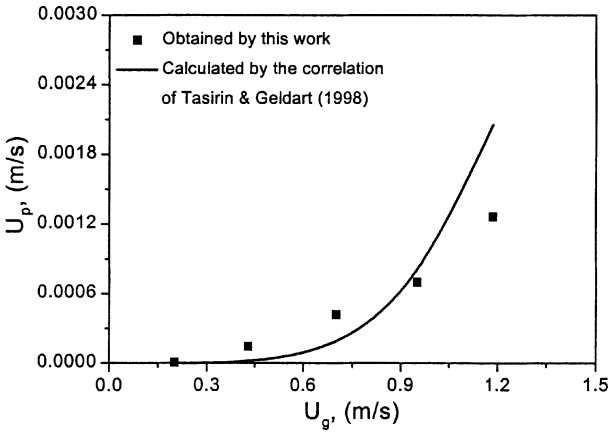

Figure 10. Particle velocity in the dispersion model.

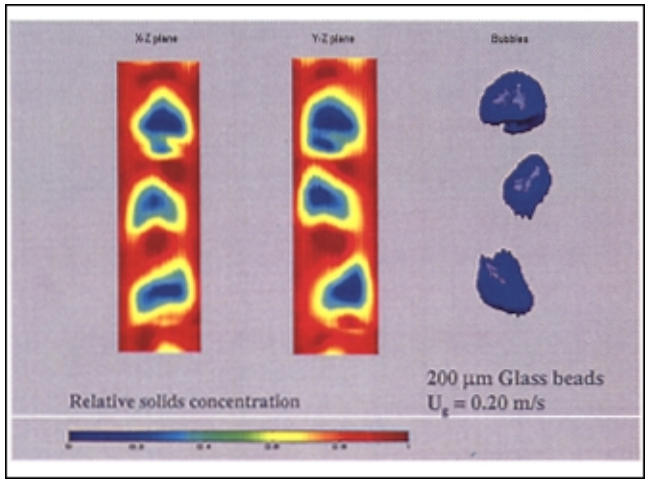

Figure 11. Images of bubbles in a gas-solid fluidized bed with 200 μm glass beads (U_g = 0.20 m/s).

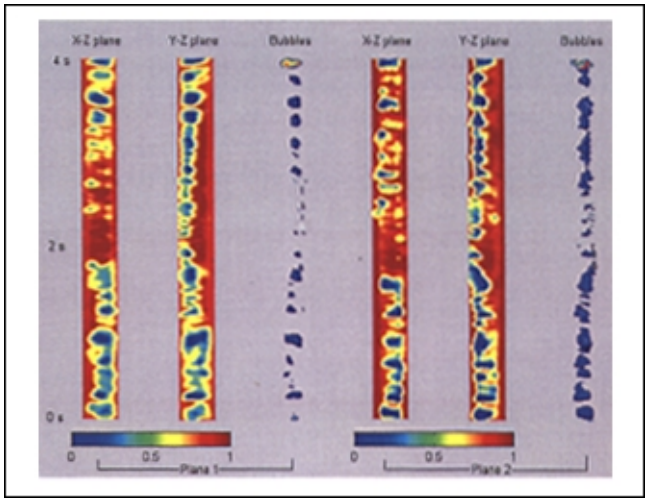

Figure 12. Quasi-3-D flow structure of a bubbling fluidized bed with FCC particles (U_g = 0.23 m/s).

is seen that the calculated values are in agreement with the averaged particle velocities obtained in this study.

Electrical capacitance tomography (ECT) measurement

The gas and solids mixing behavior in the gas-solid fluidized bed is further elaborated based on the image obtained from the ECT measurement. A column of 0.1 m ID is used for the ECT measurements. Although the bed diameter used for ECT is half of that for the mixing behavior measurement, the results obtained by the ECT are useful in the qualitative illustration of the mixing phenomena. The gas distributor is a porous plate with a pore size of 90 μm. To verify the technique under a well-established condition, the tomographic images of bubbles at a low velocity in a gas-solid fluidized bed are obtained, as shown in Figure 11. Particularly, glass beads with a diameter of 200 μm and a density of 2,500 kg/m^3 are fluidized by air at a superficial gas velocity of 0.2 m/s. The color bar in the figure corresponds to the solids concentration, spanning from low (blue) to high (red) concentrations. It is seen that bubbles have generally a spherical or ellipsoidal cap. The yellow color surrounding the bubble represents the cloud region, similar to that reported earlier by Rowe (1971). The bubble wake and drift profile are also observed as the dark red color behind the bubble in the figure. As the distance between the imaging planes 1 and 2 is 5 cm, the bubble velocity can be estimated from the bubble tracking time between these two planes and amounts to 35 cm/s for Figure 11, which is consistent with the calculated value by the equations of Kunni and Levenspiel (1991) and Cai et al. (1994).

Figure 12 shows a quasi-3-D flow behavior in a bubbling fluidized bed of FCC particles obtained by stacking 200 tomographic images of bubbles obtained in 8 s from the same plane. The FCC particles are fluidized by air at a gas velocity of 0.23 m/s. The images from two sliced sections representing the 3-D stacked gas holdup distributions at x-z and y-z planes are shown in the figure along with the quasi-3-D bubble flow. As can be seen from the figure, the bubble rises in spiral motion while rocking back and forth between the sides of the column wall. The rocking motion of the bubbles is more intensive in plane 1 than in plane 2 where the bubble motion becomes stabilized. It is observed that some regions, such as the center of the column especially in the lower plane, have fewer bubbles.

Results and Discussion

Effect of gas velocity on gas and solids dispersion

As shown in Figures 13 and 14, the flow regime has a profound effect on gas and solids dispersion in a fluidized bed. As the gas velocity increases, both the axial and radial gas dispersion coefficients increase appreciably in the bubbling regime, reach a peak at the transition velocity U_c, and then decrease sharply and level off in the turbulent regime, as shown in Figures 13a and 13b. On the other hand, both the axial and radial solids dispersion coefficients increase slightly in the bubbling regime and sharply in the turbulent regime, and then a sudden decrease when the gas velocity is beyond the transport velocity, U_{tr}, as shown in Figures 14a and 14b. The effects of the gas velocity on the gas and solids dispersion in these flow regimes are further elaborated below.

The spiral motion as well as the side-to-side rocking motion of the bubbles shown in Figure 12 contributes to the axial and radial gas dispersion in the bubbling regime. As the gas velocity increases, the bubble size increases correspondingly due to the bubble coalescence, and the motion of bubbles becomes more intense, hence, enhancing the axial and radial gas dispersion. The results are consistent with the findings of Baerns et al. (1963) and Wei et al. (1994). Baeyens and Geldart (1986) gave a good review on the mechanisms of solids mixing in the bubbling regime. For the solids dispersion in the bubbling regime, the solids in the bubble wakes and drifts are carried up to the surface, and are then dispersed by the bursting bubbles and descend to the bottom of the bed, setting up a gross circulation of solids. The solids in the bubble wakes and drifts, however, undergo local ex-

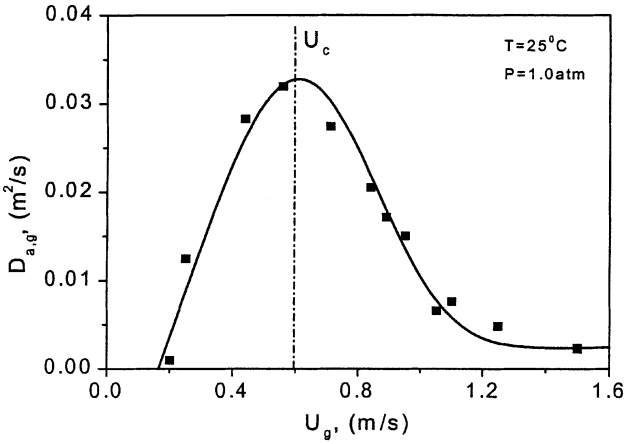

(a) Axial gas dispersion

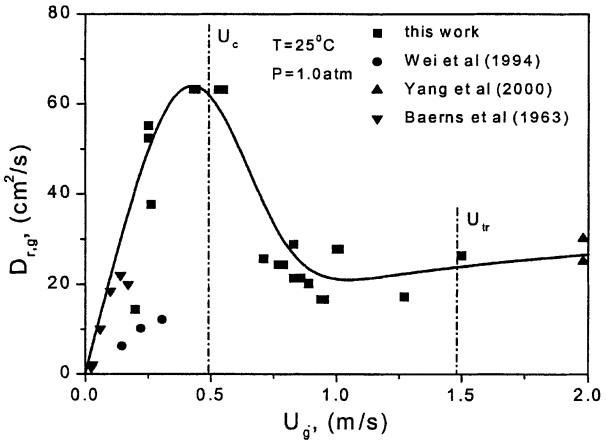

(b) Radial gas dispersion

Figure 13. Effect of U_g on axial and radial gas dispersion.

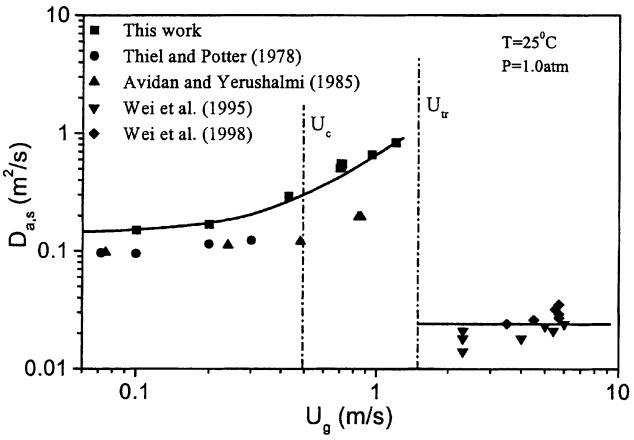

(a) Axial solids dispersion

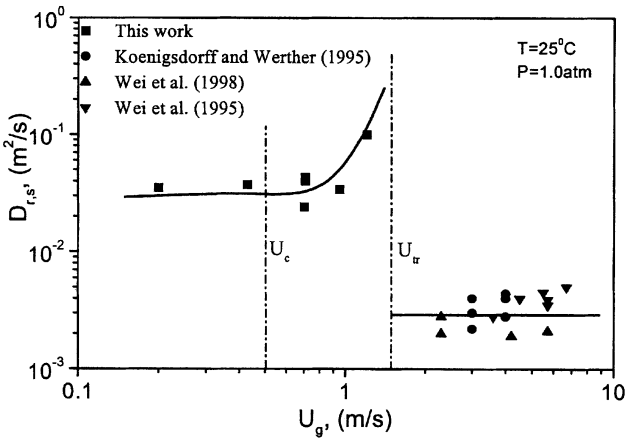

(b) Radial solids dispersion

Figure 14. Effect of U_g on axial and radial solids dispersion.

change with those in their surrounding, and the aggregated solids near the bubbles move side-to-side in the bed as the bubbles rise. This state of solids mixing characterizes the local circulation of solids. Both the gross and local circulations of solids are bubble-induced solids mixing. As these circulations increase with the gas velocity, both the axial and radial solids dispersion coefficients increase with the gas velocity. The results obtained by Thiel and Potter (1978) and Avidan and Yerushalmi (1985) also show a similar tendency; however, their values are smaller than those obtained in this study. Note that their results were obtained under the bubbling and slugging regime with different measurement techniques. Furthermore, the data of Avidan and Yerushalmi (1985) were obtained from a smaller column than the present one; their data were calibrated to the present column size using the correlation equation of Miyauchi et al. (1981) for comparison purpose.

Figure 15 shows the quasi-3-D flow behavior of the turbulent fluidized bed using the ECT for the gas velocity of 0.7 m/s. The bubble/void phase and the emulsion phase in the turbulent regime are in intermittent continuous movement (Bi et al., 2000), leading to a decrease in the axial and radial gas dispersion. The results of the axial gas dispersion are consistent with those obtained by Li and Wu (1990) in terms of axial Peclet number $Pe_{a,g}$. The standard deviations of the

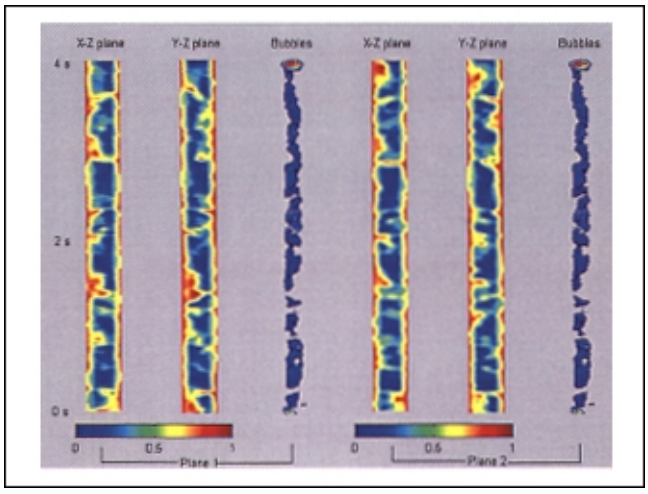

Figure 15. Quasi-3-D flow structure of a turbulent fluidized bed with FCC particles (U_g = 0.70 m/s).

tracer concentration fluctuation based on the SSHTT and of the pressure fluctuation also show a similar decreasing trend with increasing gas velocity, reflecting a similar effect due to the bubble motion on the behavior of the hydrodynamics and mixing. Cankurt and Yerushalmi (1978) and Lee and Kim (1989) obtained the similar trend of the axial dispersion coefficient in the bubbling and turbulent fluidization regimes. Lee and Kim (1989) attributed this transition phenomenon to the increase in the gas bypassing from the large bubbles in the slugging regime using glass beads with a mean diameter of 362 μm as the fluidized particles. The decrease in the gas backmixing in the turbulent regime is due to a decrease in the bubble or void size. However, for the radial dispersion coefficient, the results of Lee and Kim (1989) indicate an opposite trend in which the radial dispersion coefficient increases slightly with increasing gas velocity in the slugging regime, but sharply in the turbulent regime. The sharp increase in the turbulent regime is due to the breakup of larger slugs into the smaller bubbles. It is noted that Lee and Kim (1989) used Group B particles and the flow transition was from slugging to turbulent fluidization, while in this study, Group A particles are used and the flow transition is from bubbling to turbulent fluidization.

Both the axial and radial solids dispersion coefficients in the turbulent regime increase largely with the gas velocity, indicating a homogeneous solids phase in the bed. As shown in Figure 15, more solids around the bubble/void phase are observed to move with the bubble/void phase compared with the bubbling fluidized bed. Moreover, the intermittent movement of the clusters and voids enhances both the gross and local solids circulations in the bed. Furthermore, the movement of solids generated by the gas-particle interaction increases appreciably in the turbulent regime, compared with that in the bubbling regime. All these factors contribute to the significant solids mixing in the turbulent regime. With the increase of the gas velocity, bubble induced mixing and the mixing generated by the gas-particle interaction all increase, resulting in the increase in both the axial and radial solids dispersion coefficients. The reported experimental results on solids mixing in the turbulent regime are scarce and are all concerned with the axial mixing behavior. Utilizing a ferromagnetic tracer technique, Avidan and Yerushalmi (1985) also investigated the solids mixing of Group A particles in the turbulent fluidization regime. Their values are smaller than those obtained in this study, although of the same magnitude.

With a further increase in the gas velocity to the fast fluidization regime, the axial and radial dispersion of gas and solids in this regime has been extensively studied in the literature. The axial gas dispersion has been found to vary only slightly with the gas velocity and the solids circulating rate (Dry and Judd, 1985; Martin et al., 1992; Liu et al., 1999). The fast fluidization regime is characterized by the core-annulus structure with the dilute phase in the core region and the dense phase in the wall region. The turbulent regime is often viewed as the transition regime between the bubbling and the fast fluidization regimes. Thus, the turbulent regime would exhibit an intermediate gas mixing behavior between these two regimes. A significant decrease in the radial dispersion coefficient in the turbulent fluidized beds reflects the limitation of the radial gas transfer, which may cause nonuniformity of species in the radial direction in the bed.

Figures 14a and 14b indicate the literature results on axial and radial solids dispersion coefficients in the fast fluidization regime (Wei et al., 1995, 1998; Koenigsdorff and Werther, 1995). It is seen that the solids dispersion coefficients in the fast fluidization regime are substantially lower than those in the bubbling and turbulent regimes. For the solids dispersion coefficients in the fast fluidization regime shown in Figure 14, the bimodal RTD curves for Group A particles in a riser, including one peak detected after a few hundred milliseconds from the injection and a generally much wider peak, have been reported (Ambler et al., 1990; Wei et al., 1995). The first peak corresponds to the dispersed particles in the core region, and the second peak corresponds to the clusters in the wall region. The sudden decreases in the axial and radial solids dispersion coefficients in the fast fluidization regime are caused in part by the change in the solids flow pattern due to the flow regime change. In the bubbling and turbulent fluidization regimes, solids circulate in the bed and the net through-flow of solids is almost zero. Thus, there is only a small convection flux effect on the overall solids mixing. In the fast fluidization regime, however, there is a significant net through-flow of solids. The solids convection plays an important role in determining the solids mixing in the fast fluidization regime, leading to a relatively smaller solids dispersion in the fast fluidization regime compared to that in the bubbling and turbulent fluidization regimes.

Effect of pressure on gas and solids dispersion

At ambient temperature, the variation of the pressure from 1 to 3.1 atm has little effect on both the axial and radial gas and solids dispersion coefficients in a turbulent fluidized bed. Comprehensive reviews on the effect of pressure and temperature on gas-solid fluidization are available in the literature (Yates, 1996; Smolders and Baeyens, 2000). As the bubble size affects the dispersion and hydrodynamic behavior, it is important to examine the pressure and temperature effects on the bubble size. It is known that the bubble size for Group A particles reduces and the frequency increases with an increase in pressure (Davidson and Harrison, 1963).

In the turbulent regime, the bubble size reduction with increasing pressure has little effects on the bubble motion. Also, as the pressure increases, the gas density increases and the gas viscosity is almost unchanged. Due to the small range of pressure from 1 to 3.1 atm considered in this study, the density changes slightly yielding little effect of the pressure on the gas dispersion. The gross and local solids circulations induced by the bubble motion are not affected much by the pressure. The dispersion generated by the solids movement is directly related to the gas-particle interaction, which is dominated by the kinetic viscosity. The small variation of the kinetic viscosity with pressure leads to little effect of the pressure on the axial and radial solids dispersion. Thus, the pressure in the range considered in this study insignificantly affects the axial and radial dispersion coefficients of gas and solids for Group A particles in a turbulent fluidized bed.

Effect of temperature on gas and solids dispersion

The effect of the temperature on the gas and solids dispersion in a turbulent fluidized bed is also examined in this study

at the ambient pressure condition. The temperature varying from 25 to 435°C has little effect on the axial and radial gas and solids dispersion coefficients. The bubble size decreases with the temperature, which is reflected in the reduced amplitude of pressure fluctuations at high temperatures (Kai and Furusaki, 1985).

Similar as the effect of the pressure on the gas and solids dispersion, there is little effect of the temperature on the bubble motion due to the small effect of the bubble size reduction. The density of a gas proportionally decreases with an increase in the temperature. The viscosity of a gas increases with increasing temperature and is proportional to T^n, where n is usually between 0.5 and 1.0. The changes in density and viscosity result in a steady decrease in the Galileo number with increasing temperature. However, the temperature does not significantly alter the flow characteristics for Group A particles, as indicated by Yates (1996), and, thus, has little effect on the axial and radial gas dispersion. For the solids dispersion, the bubble-induced gross and local solids circulations do not change much with the temperature. A decrease in the density and an increase in the viscosity result in a small change in the kinetic viscosity, which leads to a nearly unvaried gas-particle interaction with increasing temperature. Thus, both the axial and radial solids dispersion generated by the solids movement are almost unchanged with the temperature. Considering the factors mentioned above, that is, the bubble size reduction, the density decrease, and the viscosity increase, the axial and radial gas and solids dispersion is only slightly affected by the temperature for Group A particles in a turbulent fluidized bed.

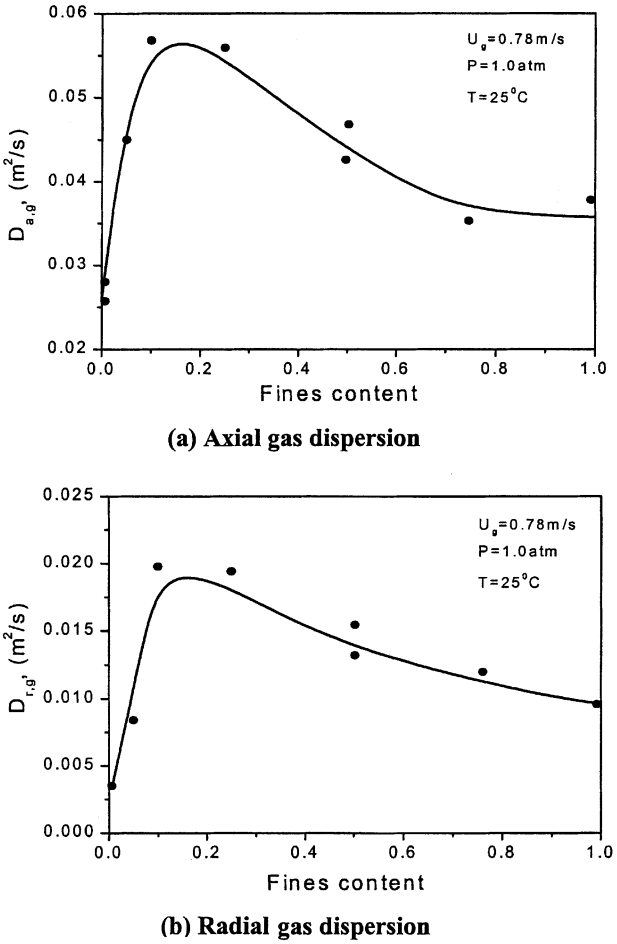

Figure 16. Effect of fines addition on axial and radial gas dispersion.

Effect of fines addition on gas and solids dispersion

Figure 16 shows the effect of the addition of fine particles on the gas dispersion in a turbulent fluidized bed at a gas velocity of 0.78 m/s at ambient temperature and pressure conditions. Figure 17 shows the effect of fines addition on the solids dispersion in a turbulent fluidized bed at a gas velocity of 0.71 m/s under ambient conditions. The addition of a small quantity of 25 μm fine particles to a 60 μm coarse particle bed yields a significant effect on the gas and solids dispersion. Both the axial and radial dispersion coefficients of gas and solids reach maximum values at a fines content of about 15%. With further addition of fine particles to the coarse particle bed, both axial and radial gas and solids dispersion coefficients decrease gradually and then level off with increasing fines content.

Comparing Figure 15 with Figure 18, the flow behavior obtained by the ECT clearly illustrates the effect of fines addition on the behavior of the bubble/void phase and the emulsion phase. The flow behavior is apparently changed at a fines content of 20%, as shown in Figure 18. Some fine particles are present at the center of the bed stimulating the breakup of the bubble/void phase. The vigorous axial and radial movement of the disintegrated bubble/void phase leads to a significant increase in the axial and radial gas dispersion coefficients. In addition, more solids are driven by the bubble/void phase to the surface of the bed, as seen in Figure 18 resulting in an increase in the gross circulation of solids. The side-to-side rocking movement of the bubble/void phase violently enhances the surrounding solids moving side-to-side. Also, the fine particles at the center of the bed may move from the core region to the wall region. These two factors lead to an increase in the local solids circulation in the bed. Because the gas velocity remains constant at 0.71 m/s, the solids dispersion generated by the solids movement due to the gas-particle interaction is nearly unvaried with the addition of fine particles. Thus, the axial and radial solids dispersion coefficients increase with the addition of a small quantity of fine particles. Upon a further increase in the fines content, however, the interactions between particles become stronger, as evidenced by particle aggregation and gradual decrease of the flowability of the emulsion phase, which contributes to the decrease in the axial and radial dispersion coefficients of the gas and solids.

Gas flux based on SSHTT

To further understand the gas mixing behavior in the bubbling and turbulent regimes, it is necessary to describe the axial and radial gas fluxes in a fluidized bed. By using the experimental results of $D_{a,g}$ and $D_{r,g}$ from the IHTT, the dimensionless tracer concentration under steady-state C/C_0

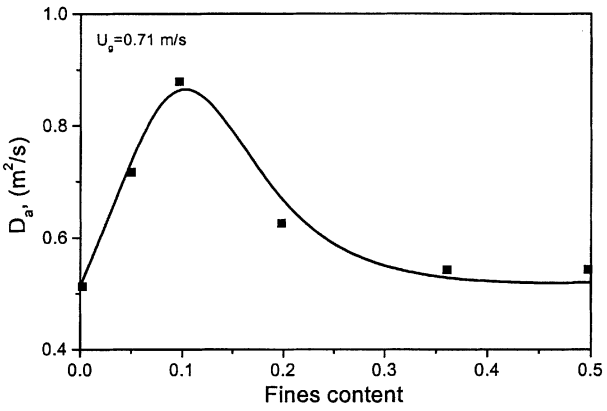

(a) Axial solids dispersion

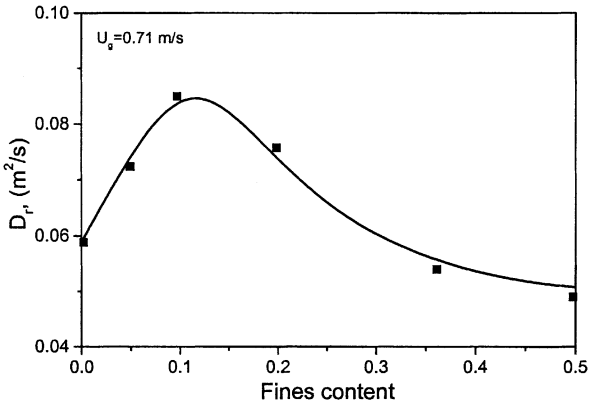

(b) Radial solids dispersion

Figure 17. Effect of fines addition on axial and radial solids dispersion.

can be calculated by Eqs. 5 and 6 based on the SSHTT. The axial convection flux, $F_{a,c,g}$, the axial dispersion flux $F_{a,d,g}$, and the radial dispersion flux $F_{r,d,g}$ of the gas can be expressed by

$$F_{a,c,g} = U_g C \tag{9}$$

$$F_{a,d,g} = -D_{a,g}\frac{\partial C}{\partial x} \tag{10}$$

$$F_{r,d,g} = -D_{r,g}\frac{\partial C}{\partial r} \tag{11}$$

The axial net gas flux $F_{a,g}$ can be given as

$$F_{a,g} = F_{a,c,g} + F_{a,d,g} \tag{12}$$

Figure 19 shows the variation of the axial and radial gas fluxes at a given concentration C_0 with the gas velocity in the core region at $r/R = 0.25$ and in the wall region at $r/R = 0.85$, respectively. Both in the core and in the wall region, the convection dominates the gas fluxes in the axial direction. In

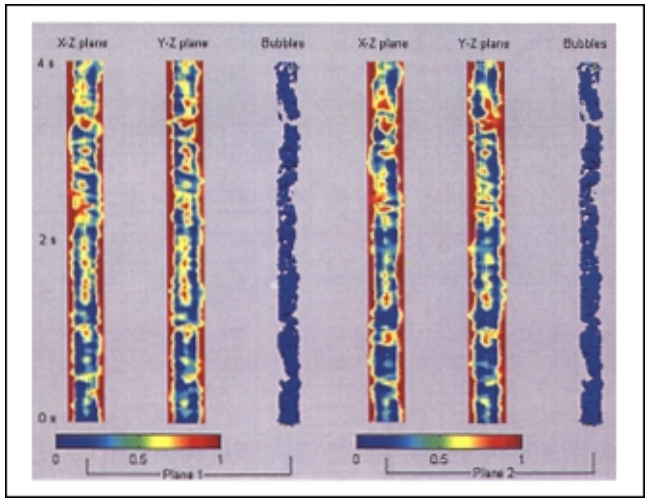

Figure 18. Quasi-3-D flow structure of a turbulent fluidized bed with 20% fine FCC addition (U_g = 0.70 m/s).

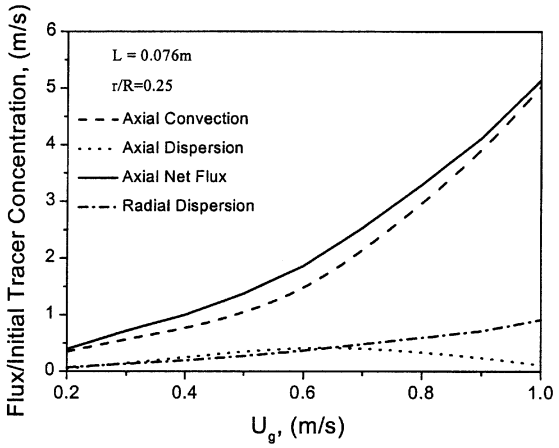

(a) In the core region

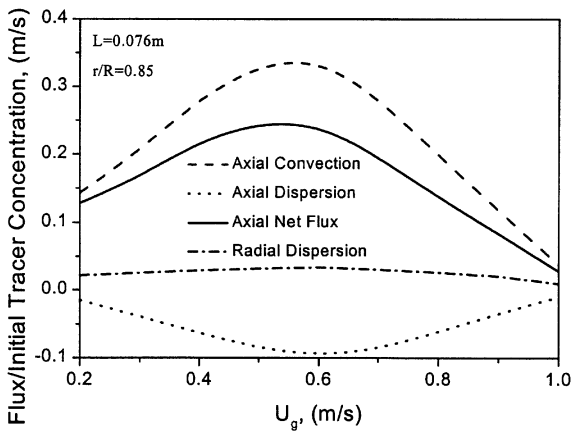

(b) In the wall region

Figure 19. Effect of U_g on axial and radial gas fluxes in the core region and wall region based on SSHTT.

the core region, the axial net flux increases slightly in the bubbling regime and largely in the turbulent regime as the gas velocity increases. However, in the wall region, the axial net flux increases initially in the bubbling regime and then decreases in the turbulent regime with increasing gas velocity. It is noted that the bubble/void phase comprising small voids and particles exists mainly in the core region of the turbulent fluidized bed. Because the axial net flux in the core region is much larger than that in the wall region, it predominates the overall axial flux in a fluidized bed. Although the axial dispersion fluxes in the core region and in the wall region are opposite, their absolute values all decrease with the gas velocity in the turbulent regime. The limited axial gas backmixing due to the particle aggregation along the column wall is reflected in the decrease in the axial dispersion flux in the wall region in a turbulent fluidized bed. The axial and radial dispersion fluxes have the same magnitude and are much smaller than the axial convection flux. It is known that the gas velocity in the radial direction is very small. Therefore, the radial convection flux can be ignored compared to the radial dispersion flux. The radial dispersion flux increases with the gas velocity in the core region, while it changes slightly in the wall region. The radial mixing is attributed to the radial dispersion flux in the core region. As the radial dispersion coefficient decreases with the gas velocity in the turbulent regime, this increase in the radial dispersion flux reflects an increase in the radial gas concentration gradients from the core to the wall regions, which is consistent with the experimental results based on the SSHTT (Figure 8).

Figure 20 illustrates the effect of fines addition on the axial and radial gas fluxes at a given concentration C_0 in a turbulent fluidized bed at a gas velocity of 0.78 m/s in the core region and the wall region, respectively. The addition of a small quantity of fine particles has a significant effect on the axial convection flux. With the addition of fine particles, the axial net flux in the core region that dominates the overall axial flux decreases sharply and then increases slightly after reaching a minimum value. It is indicated that the addition of a small quantity of fine particles renders that the whole bed behave more homogeneously and thus increases the gas mixing in the bed. The axial dispersion flux in the wall region increases in the downward direction with the addition of a small quantity of fine particles, resulting in an increase in the gas backmixing in the bed. A small quantity of fine particles decreases the radial dispersion flux in the core region. Due to the increase in the radial dispersion coefficient with the addition of a small quantity of fine particles, as shown in Figure 16, the decrease in the radial dispersion flux implies a decrease in the radial gas concentration gradients from the core to the wall regions.

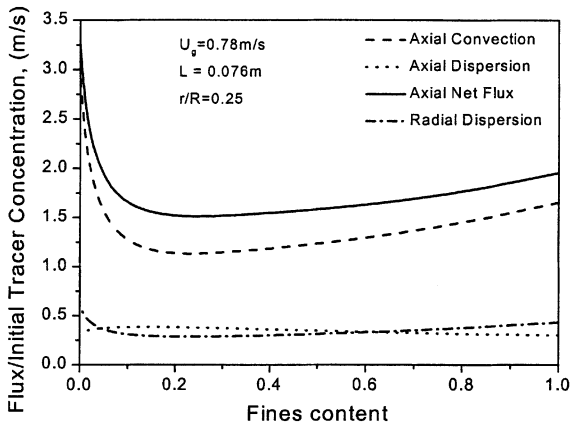

(a) In the core region

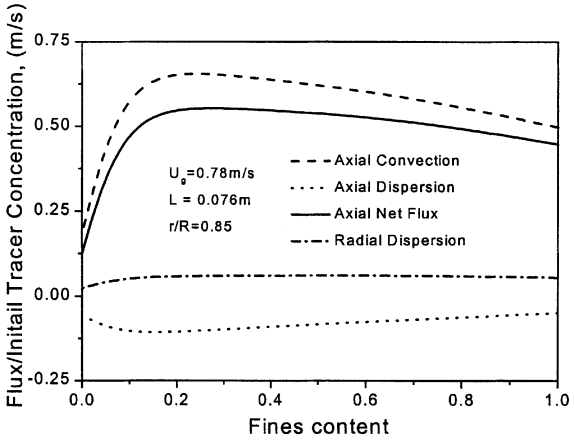

(b) In the wall region

Figure 20. Effect of fines addition on axial and radial gas fluxes in the core region and wall region based on SSHTT.

Solids flux based on IPTT

By using the experimental results of $D_{a,s}$ and $D_{r,s}$ from the IPTT, the dimensionless tracer concentration C/C_0 at a given time can be calculated by Eq. 8. The expressions of the axial convection flux $F_{a,c,s}$, the axial dispersion flux $F_{a,d,s}$, the radial dispersion flux $F_{r,d,s}$, and the axial net flux $F_{a,s}$ of the solids are the same as those defined for the gas. The notations for the gas, that is, U_g, $D_{a,g}$, and $D_{r,g}$, are replaced by those for the solids, that is, U_p, $D_{a,s}$, $D_{r,s}$, respectively.

Figure 21 illustrates the axial and radial solids fluxes at a time of 0.1 s and a given concentration C_0, varying with the gas velocity in the core region and in the wall region, respectively. Because the axial U_p is small, as shown in Figure 10, and the radial particle velocity can be ignored, the dispersion fluxes dominate the overall fluxes in both the axial and radial directions. The axial and radial solids dispersion fluxes in the core region are of the same order of magnitude as those in the wall region in the turbulent regime. The axial dispersion flux is one order of magnitude higher than the radial dispersion flux. As the gas velocity increases, the axial and radial dispersion fluxes in both the core region and the wall regions decrease slightly in the bubbling regime and largely in the turbulent regime, which corresponds to the increase in the solids dispersion coefficients with the gas velocity, as seen in Figure 14.

Figure 22 shows the effect of fines addition on the axial and radial solids fluxes at a time of 0.1 s and a given concentration C_0 in a turbulent fluidized bed at a gas velocity of 0.71 m/s in the core region and in the wall region, respectively. There is nearly no variation in the axial convection due to the fixed gas velocity. Both the axial and radial solids fluxes

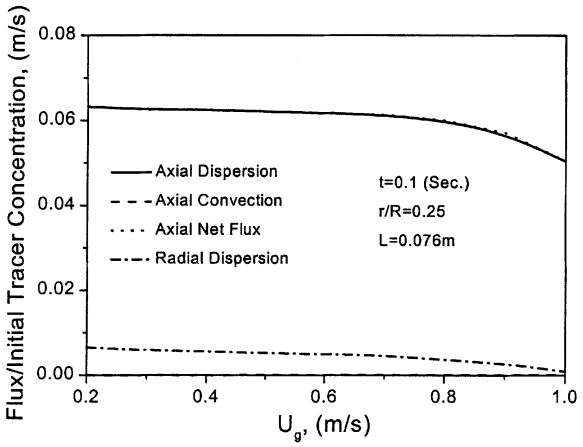

(a) In the core region

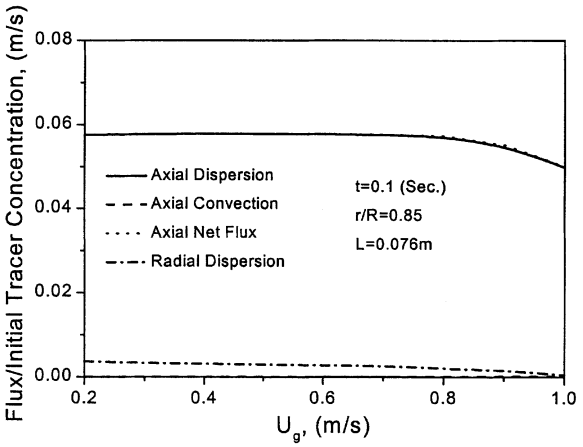

(b) In the wall region

Figure 21. Effect of U_g on axial and radial solids fluxes in the core region and wall region based on IPTT.

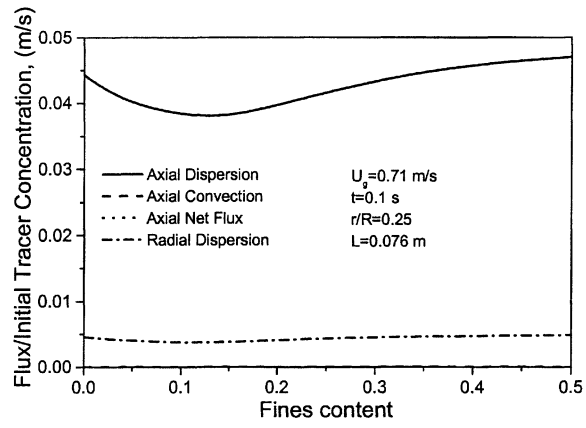

(a) In the core region

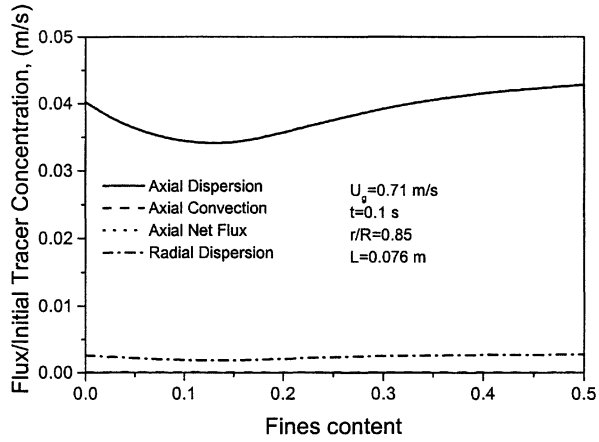

(b) In the wall region

Figure 22. Effect of fines addition on axial and radial solids fluxes in the core region and wall region based on IPTT.

initially decrease sharply and then increase gradually with increasing fines content. The addition of a small quantity of fine particles has a significant effect on the axial dispersion flux and a relatively small effect on the radial dispersion flux. In both the core region and wall region, the axial and radial dispersion fluxes reach the minimum values at a fines content of about 15%, which corresponds to the maximum values of the solids dispersion coefficients shown in Figure 17.

Concluding Remarks

The helium and phosphor tracer techniques are respectively used to investigate the gas and solids mixing behavior in both the bubbling and turbulent gas-solid fluidized beds. Electrical capacitance tomography is applied to examine the real time, quasi-3-D flow behavior in the bed. Both the axial and radial dispersion behavior in the bubbling, turbulent, and fast fluidization regimes are analyzed. The variation of the axial and radial gas dispersion coefficients with the gas velocity is found to reach a maximum at the transition velocity U_c. In the turbulent regime, the solids dispersion coefficients are much higher than those in the other two regimes. Temperature and pressure have little effect on the axial and radial dispersion of gas and solids. A small quantity of fine particles greatly affects both the axial and radial mixing behavior of gas and solids. Based on the flux analyses, the axial gas flux is dominated by the convection, while the dispersion dominates the solids fluxes in both axial and radial directions. The flow behavior obtained by the ECT clearly illustrates the disintegration of the bubble/void phase due to the fines addition in the turbulent fluidized bed.

Notation

C = tracer concentration, kg/m^3
C_0 = initial tracer concentration, kg/m^3
D = bed diameter, m
D_a = axial dispersion coefficient, m^2/s
D_r = radial dispersion coefficient, m^2/s
F_a = axial net flux, kg/m$^2\cdot$s
$F_{a,c}$ = axial convection flux, kg/m$^2\cdot$s
$F_{a,d}$ = axial dispersion flux, kg/m$^2\cdot$s
$F_{r,d}$ = radial dispersion flux, kg/m$^2\cdot$s

$Pe_{a,g}$ = axial Peclet number of gas, $= LU_g/D_{a,g}$
U_c = transition velocity from the bubbling to turbulent regimes, m/s
U_g = superficial gas velocity, m/s
U_p = tracer particle velocity, m/s
U_{tr} = transport velocity from the turbulent to fast fluidization regimes, m/s
V_g = tracer gas velocity, m/s
β_n = n-th positive root of zero order Bessel function
φ = dimensionless velocity, $\varphi = (U \cdot R)/(2\sqrt{D_a D_r})$ (for gas, $U = V_g$ or U_g, for solids $U = U_p$)
θ = dimensionless time, $\theta = D_r t/R^2$
ξ = dimensionless axial position, $\xi = (x\sqrt{D_r})/(R\sqrt{D_a})$
ρ = reduced radial position, $\rho = r/R$

Subscripts

g = gas phase
s = solids phase

Literature Cited

Ambler, P. A., B. J. Milne, F. Berruti, and D. S. Scott, "Residence Time Distribution of Solids in a Circulating Fluidized Bed: Experimental and Modeling Studies," *Chem. Eng. Sci.*, **45**, 2179 (1990).

Avidan, A., and J. Yerushalmi, "Solids Mixing in an Expanded Top Fluid Bed," *AIChE J.*, **31**, 835 (1985).

Baerns, M., F. Fetting, and K. Schugerl, "Communications on Fluidized Beds. V. Radial and Axial Gas Mixing in Fluidized Beds," *Chem. Ing. Tech.*, **35**, 609 (1963).

Baeyens, J., and D. Geldart, "Solids Mixing," *Gas Fluidization Technology*, D. Geldart, ed., Wiley-Interscience Publication, Chichester, England, p. 97 (1986).

Beck, M. S., and R. A. Williams, "Process Tomography: a European Innovation and its Application," *Meas. Sci. Technol.*, **7**, 215 (1996).

Bi, H. T., N. Ellis, I. A. Abba, and J. R. Grace, "A State-of-the-Art Review of Gas-Solid Turbulent Fluidization," *Chem. Eng. Sci.*, **55**, 4789 (2000).

Cai, P., S. P. Chen, Y. Jin, Z. Q. Yu, and Z. W. Wang, "Effect of Operating Temperature and Pressure on the Transition from Bubbling to Turbulent Fluidization," *AIChE Symp. Series*, **270**, 37 (1989).

Cai, P., Y. Jin, Z. Q. Yu, and L. S. Fan, "Mechanistic Model for Onset Velocity Prediction for Regime Transition from Bubbling to Turbulent Fluidization," *Ind. Eng. Chem. Res.*, **31**, 632 (1992).

Cai, P., M. Schiavetti, G. DeMichele, G. C. Grazzini, and M. Miccio, "Quantitative Estimation of Bubble Size in PFBC," *Powder Technol.*, **80**, 99 (1994).

Cankurt, N. T., and J. Yerushalmi, "Gas Backmixing in High Velocity Fluidized Bed," *Fluidization*, J. F. Davidson and D. L. Keairns, eds., Cambridge University Press, Oxford, p. 307 (1978).

Davidson, J. F., and D. Harrison, *Fluidized Particles*, Cambridge University Press, Cambridge (1963).

Dry, R. J., and M. R. Judd, "Fluidized Beds of Fine, Dense Powders: Scale-up and Reactor Modeling," *Powder Technol.*, **43**, 41 (1985).

Dyakowski, T., L. Jeanmeure, and A. Jaworski, "Applications of Electrical Tomography for Gas-Solids and Liquid-Solids Flows—a Review," *Powder Technol.*, **112**, 174 (2000).

Dyakowski, T., R. B. Edwards, C. G. Xie, and R. A. Williams, "Application of Capacitance Tomography to Gas-Solid Flows," *Chem. Eng. Sci.*, **52**, 2099 (1997).

Foka, M., J. Chaouki, C. Guy, and D. Klvana, "Gas Phase Hydrodynamics of a Gas-Solid Turbulent Fluidized Bed Reactor," *Chem. Eng. Sci.*, **51**, 713 (1996).

George, D. L., J. R. Torczynski, K. A. Shollenberger, T. J. O'Hern, and S. L. Ceccio, *Quantitative Tomographic Measurements of Opaque Multiphase Flows*, Sandia Report SAND2000-0441, Sandia National Laboratories, Albuquerque, NM (2000).

Kai, T., and S. Furusaki, "Behavior of Fluidized Beds of Small Particles at Elevated Temperatures," *J. of Chem. Eng. of Japan*, **18**, 113 (1985).

Klinkenberg, A., H. J. Krajenbrink, and H. A. Lauwerier, "Diffusion in a Fluid Moving at Uniform Velocity in a Tube," *Ind. and Eng. Chemistry*, **45**, 1202 (1953).

Koenigsdorff, R., and J. Werther, "Gas and Solids Mixing in and Flow Structure Modeling of the Upper Dilute Zone of a Circulating Fluidized Bed," *Powder Technol.*, **82**, 317 (1995).

Kumar, S. B., D. Mosleman, and M. P. Dudukovic, "Gas-Holdup Measurements in Bubble Columns Using Computed Tomography," *AIChE J.*, **43**, 1414 (1997).

Kunni, D., and O. Levenspiel, *Fluidization Engineering*, 2nd ed., Butterworth-Heinemann, Boston (1991).

Lee, G. S., and S. D. Kim, "Axial Mixing of Solids in Turbulent Fluidized Beds," *Chem. Eng. J.*, **44**, 1 (1990).

Lee, G. S., and S. D. Kim, "Gas Mixing in Slugging and Turbulent Fluidized Beds," *Chem. Eng. Comm.*, **86**, 91 (1989).

Li, J., and H. Weinstein, "An Experimental Comparison of Gas Backmixing in Fluidized Beds Across the Regimes Spectrum," *Chem. Eng. Sci.*, **44**, 1697 (1989).

Li, Y., and P. Wu, "A Study on Axial Gas Mixing in a Fast Fluidized Bed," *Circulating Fluidized Bed Technology III*, P. Basu, M. Horio and M. Hasatani, eds., Pergamon, Oxford, p. 581 (1990).

Liu, J., J. R. Grace, H. Bi, H. Morikawa, and J. Zhu, "Gas Dispersion in Fast Fluidization and Dense Suspension Upflow," *Chem. Eng. Sci.*, **54**, 5441 (1999).

Martin, M. P., P. Turlier, J. R. Bernard, and G. Wild, "Gas and Solid Behavior in Cracking Circulating Fluidized Beds," *Powder Technol.*, **70**, 249 (1992).

Miyauchi, T., S. Furusaki, S. Morooka, and Y. Ikeda, "Transport Phenomena and Reaction in Fluidized Catalyst Beds," *Adv. Che. Eng.*, **11**, 275 (1981).

Mostoufi, N., and J. Chaouki, "Local Solid Mixing in Gas-Solid Fluidized Beds," *Powder Technol.*, **114**, 23 (2001).

Rowe, P. N., "Experimental Properties of Bubbles," *Fluidization*, J. F. Davidson and D. Harrison, eds., Academic Press, New York, p. 121 (1971).

Smolders, K., and J. Baeyens, "Fluidization at Elevated Temperature and/or Pressure," *Powder Handl. Process.*, **12**, 47 (2000).

Smolders, K., D. Geldart, and J. Bacyens, "The Physical Models of Cyclone Diplegs in Fluidized Beds," *Chinese J. of Chem. Eng.*, **9**, 337 (2001).

Sun, G. L., and J. R. Grace, "The Effect of Particle-Size Distribution on the Performance of a Catalytic Fluidized-Bed Reactor," *Chem. Eng. Sci.*, **45**, 2187 (1990).

Tasirin, S. M., and D. Geldart, "Entrainment of FCC from Fluidized Beds—a New Correlation for the Elutriation Rate Constants $K_{i\infty}^*$," *Powder Technol.*, **95**, 240 (1998).

Thiel, W. J., and O. E. Potter, "The Mixing of Solids in Slugging Gas Fluidized Beds," *AIChE J.*, **24**, 561 (1978).

Warsito, W., and L.-S. Fan, "Neural Network Based on Multi-Criteria Optimization Image Reconstruction Technique for Imaging Two- and Three-Phase Flow Systems Using Electrical Capacitance Tomography," *Measurement Sci. and Technol.*, **12**, 2198 (2001).

Warsito, W., M. Ohkawa, N. Kawata, and S. Uchida, "Cross-Sectional Distributions of Gas and Solid Holdups in Slurry Bubble Column Investigated by Ultrasonic Computed Tomography," *Chem. Eng. Sci.*, **54**, 4711 (1999).

Wei, F., W. Chen, Y. Jin, and Z. Q. Yu, "Lateral and Axial Mixing of the Dispersed Particles in CFB," *J. of Chem. Eng. of Japan*, **28**, 506 (1995).

Wei, F., F. Lu, Y. Jin, and Z. Yu, "Study on the Behavior of Gas Mixing in Gas-Solid Fluidized Bed with Composite Distributor," *Shiyou Huagong* (in Chinese), **23**, 631 (1994).

Wei, F., S. Lin, and G. Yang, "Gas and Solids Mixing in a Commercial FCC Regenerator," *Chem. Eng. Technol.*, **16**, 109 (1993).

Wei, F., Y. Cheng, Y. Jin, and Z. Q. Yu, "Axial and Lateral Dispersion of Fine Particles in a Binary-Solid Riser," *Can. J. of Chem. Eng.*, **76**, 19 (1998).

Yang, W. Q., and S. Liu, "Role of Tomography in Gas/Solids Flow Measurement," *Flow Measurement and Instrumentation*, **11**, 237 (2000).

Yang, Y. L., Y. Jin, Z. Q. Yu, J. X. Zhu, and H. T. Bi, "Local Slip Behaviors in the Circulating Fluidized Bed," *AIChE Symp. Ser.*, **296**, 81 (1993).

Yates, J. G., "Effects of Temperature and Pressure on Gas-Solid Fluidization," *Chem. Eng. Sci.*, **51**, 167 (1996).

Manuscript received Aug. 8, 2001, and revision received Feb. 25, 2002.